Reac Kinet Mech Cat (2017) 121:645–655
DOI 10.1007/s11144-017-1188-9

Optimization of cesium and potassium promoter loading in alkali-doped $Zn_{0.4}Co_{2.6}O_4|Al_2O_3$ catalysts for N_2O abatement

Klaudia Ciura[1] · Gabriela Grzybek[1] · Sylwia Wójcik[1] · Paulina Indyka[1] · Andrzej Kotarba[1] · Zbigniew Sojka[1]

Received: 2 March 2017 / Accepted: 13 April 2017 / Published online: 26 April 2017

Abstract A series of potassium or cesium doped $Zn_{0.4}Co_{2.6}O_4|Al_2O_3$ catalysts with different alkali loadings were prepared, characterized with respect to chemical composition (XRF), structure (XRD, RS) morphology (TEM), and the alkali promoter thermal stability. A strong beneficial effect on the deN_2O activity of the $Zn_{0.4}Co_{2.6}O_4|Al_2O_3$ catalyst (decrease in the $T_{50\%}$ by about 80 °C) was observed for both promoters at different surface coverages. It was found that in comparison to a rather narrow range of optimal cesium loading (0.5–2 atoms/nm^2) a comparable promotional effect of potassium doping was observed for a slightly wider surface concentrations (0.5–3 atoms/nm^2). Such difference was attributed to surface dispersion of potassium over the alumina support and the spinel active phase, while cesium was found to be located mainly on the spinel phase. For practical applications, the superiority of potassium over cesium consist in fact that a similar beneficial effect is associated with much higher thermal stability in the temperature range of the catalyst deN_2O operation and lower price of the promoter precursor.

Keywords Alkali promotion · Decomposition of nitrous oxide · Supported catalyst · Cobalt spinel · Co_3O_4

Introduction

Nitrous oxide is commonly recognized as an important greenhouse gas, emitted from natural (nitrogen cycles) and anthropogenic (mainly nitric and adipic acid production) sources. The N_2O emission represents 6% of the total greenhouse gas emission. However, its global warming potential (GWP) is 310 and 21 times higher than for CO_2 and CH_4, respectively [1]. Moreover, the presence of this gas in the

✉ Gabriela Grzybek
g.grzybek@uj.edu.pl

[1] Faculty of Chemistry, Jagiellonian University, Ingardena 3, 30-060 Krakow, Poland

atmosphere leads to destruction of the ozone layer [2]. Thus, decomposition of N_2O into N_2 and O_2 has developed recently into a topic of a vital interest for environmental catalytic chemistry.

Some of the most efficient catalysts for N_2O abatement are based on cobalt spinel [3, 4]. The catalytic performance of Co_3O_4 can be modified by bulk doping with transition metal cations (such as Zn, Ni, Cu, Mn, Fe) [5–10] and surface doping with alkali dopants (Na, K, Cs) [3, 8, 11–13]. Addition of alkali results in a substantial lowering of the reaction temperature window, making such catalytic system potentially suitable for the low temperature deN_2O process [11]. The beneficial effect of alkali promoters has been reported to be mainly of an electronic origin [14, 15]. The presence of alkali promoters on the catalyst surface lowers the work function of the cobalt spinel facilitating redox processes that occur between the catalyst surface and the N_2O reactant. It also stimulates recombination of surface oxygen intermediates, closing the catalytic cycle [11, 12]. The positive role of the alkali promoters in enhancement of the Co_3O_4 activity increases in the order: $Na < K < Cs$, and exhibits a strongly non-monotonous character as a function of surface coverage [11, 12, 16]. Among them, potassium and cesium are the most often investigated due to their strongest promotional effects. Beside the positive role in the activity enhancement the thermal stability of the alkali promoters play an important role for a long time-on-stream operation of the catalyst. The nature of the counter anion also plays an important role in the promotion of the catalytic activity of N_2O decomposition. In the particular case of potassium, it has been found that the promotional effect strongly depends on the precursor nature (K_2CO_3, KNO_3, CH_3COOK, KOH), and the highest activity was observed for K_2CO_3. It has been assigned to the best surface dispersion and thermal stability of the potassium promoter [16].

It has been found previously by us that the synergetic effect of double promotion of cobalt spinel by Zn (bulk) and K (surface) led to spectacular decrease in the temperature of 50% N_2O conversion by 200 °C [17]. However, despite such promising performance in the N_2O decomposition reaction, the development of an industrial scale catalyst based on Co_3O_4 as a bulk active phase was hindered by the unsatisfactory mechanical stability of the catalyst extrudates and by the high price of cobalt as well. These problems can be solved quite readily by the dispersion of cobalt spinel active phase on a shaped support such as alumina, silica, magnesia or ceria [4, 18–22]. However, since the alkali promoter loading is crucial for the deN_2O performance of the catalyst, and both the under- and the over-doping lead to pronounced deterioration of the activity, the alkali promotion level must be carefully adjusted for a given catalyst. This problem is becoming more subtle in the case of supported catalysts, since the promoter may be dispersed not only on the active phase but also on the carrier surface [8]. To resolve this problem, a series of potassium and cesium doped supported $Zn_{0.4}Co_{2.6}O_4|Al_2O_3$ catalysts was prepared and tested in the N_2O decomposition. The optimal range of surface K and Cs loadings and their thermal stability were determined and discussed in terms of the potential applicability in a large scale preparation practice.

Experimental

Catalyst preparation

The alpha-alumina support, prepared from commercial powder pseudoboehmite (Sasol Versal) by calcination at 1400 °C for 4 h, was supplied by the Institute of New Chemical Syntheses (INS Puławy, Poland). The supported catalyst with 15% loading of the active phase $Zn_{0.4}Co_{2.6}O_4$ was prepared by the incipient wetness impregnation of the α-alumina support with the use of a 30 vol% glycerol-aqueous solution of 4.49 M $Co(NO_3)_2$ (AKTYN, pure p.a.) and 0.69 M $Zn(NO_3)_2$ (Dorchem, pure p.a.) [23]. The obtained sample was dried at 120 °C for 1 h, and then calcined at 500 °C for 4 h. The catalyst was next doped with alkali (K or Cs) by incipient wetness impregnation with an aqueous solution of K_2CO_3 (POCH, pure p.a.) or Cs_2CO_3 (Aldrich) with concentrations corresponding to the surface loadings of potassium and cesium in the range of 0–10 atoms K/nm^2 and 0–6 atoms Cs/nm^2 [4, 8, 11, 12]. Then, the cycle of drying and calcination was repeated. The samples were labeled according to the content and kind of the alkali dopant (Table 1) [12].

Catalysts characterization

The BET surface area of undoped catalysts was determined by nitrogen adsorption at −196 °C in an automatic volumetric system (Autosorb-6, Quantachrome) and was equal to 8 m^2 g^{-1}.

The loading of the alkali promoter was determined using an energy-dispersive XRF spectrometer (Thermo Scientific, ARL QUANT'X) equipped with Rh anode

Table 1 The nominal and experimental (determined by XRF method) content of potassium or cesium in the doped $Zn_{0.4}Co_{2.6}O_4|Al_2O_3$ catalysts

Sample label (atoms per nm^2)	Nominal content/wt%	Experimental (atoms per nm^2)	Experimental content/wt%
0.5 K	0.026	0.37	0.038
1 K	0.052	0.65	0.067
1.5 K	0.078	1.52	0.079
2 K	0.104	2.24	0.116
2.5 K	0.130	2.60	0.135
5 K	0.260	5.44	0.282
10 K	0.518	11.02	0.571
0.5 Cs	0.088	0.15	0.027
1 Cs	0.177	0.49	0.086
2 Cs	0.353	1.90	0.335
4 Cs	0.706	4.24	0.749
6 Cs	1.060	6.28	1.110

The bold values in the first column are the nominal alkali promoter concentrations expressed as alkali atoms per nm^2. These values were used as the samples labels

(which generates X-rays in the range of 4–50 kV with 1 kV step and a 1 mm beam size), and with a 3.5 mm Si(Li) drifted crystal detector operated with a Peltier cooling. For quantitative analysis, a series of metallic calibration standards and the UniQuant software were used.

X-ray diffraction measurements were carried out by Rigaku MiniFlex diffractometer with Cu K_α radiation at 10 mA and 10 kV. The diffractograms were recorded in a 2θ range from 10° to 90° with the 0.02° step, and the counting time of 1 s per step. The diffractograms were indexed using the ICSD database.

The phase composition and structure verification were examined by Raman spectroscopy using a Renishaw InVia spectrometer with a confocal Leica DMLM microscope and a CCD detector with the excitation wavelength of 785 nm. The Raman scattered light was collected in the spectral range of 100–900 cm^{-1} with a resolution of 1 cm^{-1}. At least five scans were accumulated to ensure a sufficient signal to noise ratio.

TEM observations were carried out by means of a FEI Tecnai Osiris microscope with an X-FEG Schottky field emitter operated at 200 kV. The instrument was also equipped with a Super-X EDX (energy dispersive X-ray) windowless detector system with a 4-sector silicon drift detector (SDD). The Z-contrast images were acquired using a high angle annular dark field (HAADF) detector in the scanning mode. HAADF-STEM images coupled with EDX elemental mapping were acquired using Bruker Esprit software for the sample drift correction. For the microscopic measurements the samples were deposited on a lacey carbon-coated copper grid.

The stability of potassium and cesium was investigated by the species resolved – thermal alkali desorption (SR–TAD) method [24]. The experiments were carried out in a vacuum apparatus with a background pressure of 10^{-8} mbar. The samples, in the form of wafers of 13 mm in diameter with a mass of about 100 mg, were heated from 25 to 600 °C. The desorption flux of alkali atoms, *S*/pA, was determined by means of a surface ionization detector. During the measurements, the samples were biased with a positive potential +5 V to suppress thermionic emission of electrons. The resultant positive current was measured directly with a digital electrometer (Keithley 6512), and averaged over four independent data points for each temperature. The activation energy (E_{des}) for alkali desorption was calculated with an assumption that the process follows first order kinetics by applying Arrhenius equation justified elsewhere [25].

Catalytic tests

Catalytic tests of nitrous oxide decomposition were carried out for all catalysts in a temperature programmed surface reaction (TPSR) mode. A 300 mg sieve fraction of the catalyst (0.2–0.3 mm) was placed in a quartz flow reactor, with a thermocouple positioned just above the catalyst bed. The reaction was performed in the temperature range of 20–600 °C (with a heating rate of 10°/min) and at the atmospheric pressure, using a gas mixture of 5% N_2O in He with the total gas flow of 30 ml/min (GHSV = 7000 h^{-1}; calculated for catalyst volume). Before measuring the catalysts activity, the samples were pretreated in situ by heating up to 600 °C. Changes in the gas composition were monitored by a quadrupole mass

spectrometer (RGA200, SRS, lines $m/z = 44$ (N_2O), 32 (O_2), 30 (NO), 28 (N_2), 18 (H_2O)).

Results and discussion

The synthesized catalysts were examined with respect to the spinel active phase formation (XDR, Raman spectroscopy), spinel and alkali loading (XRF), their morphology including alkali distribution mapping (TEM/EDX) and thermal stability of the alkali promoters (SR-TAD). The XRF analysis of the investigated samples indicated the presence of 17.7 wt% of the spinel $Zn_{0.4}Co_{2.6}O_4$ phase, close to the intended loading of 15 wt%. The alkali content, which was the main optimization parameter in this study, is summarized in Table 1.

The crystalline structure of the active phase of the supported catalyst was examined by XRD and Raman techniques. A typical XRD pattern of the 2K-$Zn_{0.4}Co_{2.6}O_4|Al_2O_3$ catalyst is shown in Fig. 1, as an example. Apart from the dominant diffraction peaks due to the α-Al_2O_3 support, several weaker diffraction lines at $2\Theta = 31.3°$; 36.9°; 44.9°; 55.7°; 59.5°; 65.4°, corresponding to the (220), (311), (400), (422), (511) and (440) reflection planes of the cobalt spinel phase, are clearly visible [8]. No apparent changes in the XRD patterns were observed upon alkali doping of the samples, indicating that the spinel active phase remains essentially intact upon the alkali promotion.

Raman spectra of the investigated catalysts are shown in Fig. 2. Five bands located at 195 (F_{2g}), 487 (E_g), 526, 624 (F_{2g}) and 694 (A_{1g}) cm^{-1} confirmed the presence of the spinel phase, and absence of any impurities [26]. The apparent asymmetry of the Raman A_{1g} and F_{2g} peaks is a result of substitution of the zinc for cobalt in the Co_3O_4 framework, implying formation of the intended $Zn_xCo_{(1-x)}$-Co_2O_4 solid solution [17]. As a result, analysis of the XRD and RS data eliminates a possibility of undesired ZnO segregation from the spinel active phase. In the case of

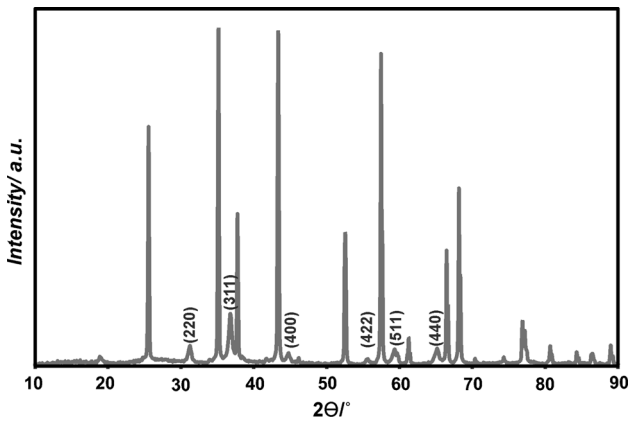

Fig. 1 XRD pattern of 2K-$Zn_{0.4}Co_{2.6}O_4|Al_2O_3$ catalyst

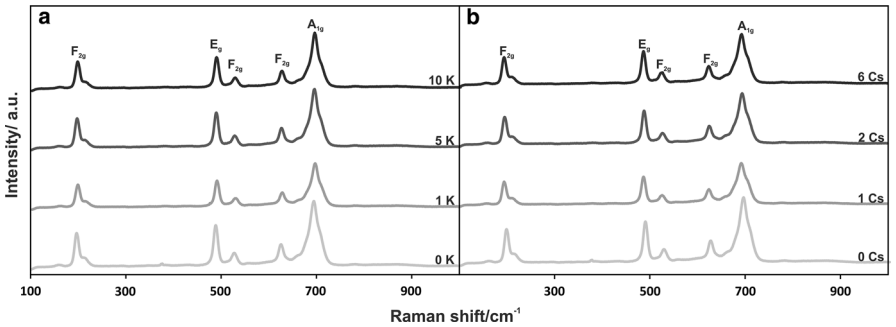

Fig. 2 Raman spectra of $Zn_{0.4}Co_{2.6}O_4|Al_2O_3$ catalyst doped by **a** K and **b** Cs

alkali-doped catalysts there is no difference observed on Raman spectra in comparison with the un-doped samples as it was previously observed [8].

STEM-HAADF images of the alkali promoted catalysts show the dispersion of the spinel nanocrystals over the alumina micrograins (Figs. 3a$_1$ and 3b$_1$). The Al_2O_3 grains of a rounded shape and $\sim$0.5–2 μm in size are decorated by the $Zn_{0.4}Co_{2.6}O_4$ spinel nanocrystals. A detailed inspection of the catalyst nanostructure of the

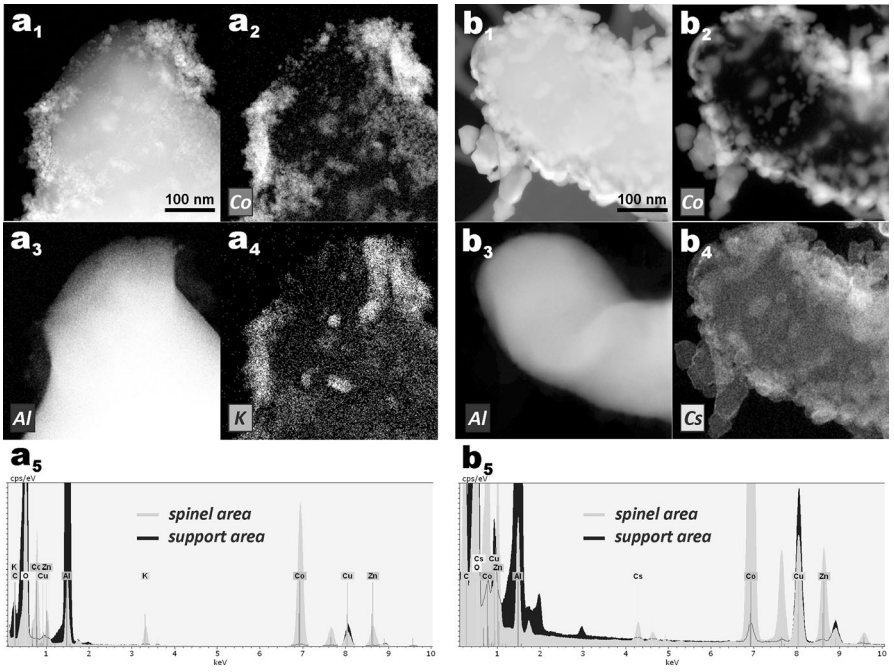

Fig. 3 STEM-HAADF images for: **a$_1$** K-$Zn_{0.4}Co_{2.6}O_4|Al_2O_3$ calcined at 500 °C, **b$_1$** Cs-$Zn_{0.4}Co_{2.6}O_4|Al_2O_3$ calcined at 500 °C. HAADF Z-contrast images showing the size and distribution of the spinel nanocrystals over larger grains of Al_2O_3 support. The corresponding EDX spectra (**a$_5$** and **b$_5$**) along with the associated EDX chemical maps (**a$_2$**–**a$_4$** and **b$_2$**–**b$_4$**) showing element repartition between the Al_2O_3 support and $Zn_{0.4}Co_{2.6}O_4$ spinel active phase

potassium/cesium-promoted $Zn_{0.4}Co_{2.6}O_4|\alpha\text{-}Al_2O_3$ catalysts showed that the typical spinel crystallites exhibit polyhedral shape (faceted) with the dominant (100) and (111) terminations as revealed by the image analysis and inverse Wulff construction [23]. The spinel active phase is fairly well dispersed over the alumina carrier, and the average size of the $Zn_{0.4}Co_{2.6}O_4$ crystallites is distinctly smaller for the potassium-doped samples (10–20 nm) in comparison to the cesium-promoted catalyst (40–50 nm). The spinels nanograins are both directly attached to the alumina support surface or connected to another nanograins by forming small aggregates (Figs. $3a_1$ and $3b_1$).

The presence of the alkali promoter (potassium or cesium) on the $Zn_{0.4}Co_{2.6}O_4|Al_2O_3$ catalyst was confirmed by the STEM-EDX measurements. Figs. $3a_5$ and $3b_5$ show the corresponding EDX spectra with the well-developed signals characteristic for potassium (K_α at 3.31 eV and K_β at 3.59 eV) and for cesium (L_α at 4.28 eV, $L_{\beta1}$ at 4.62 eV, $L_{\beta2}$ at 4.93 eV). The STEM-EDX elemental mapping revealed apparent differences in the alkali surface redistribution between the spinel and the support (Figs. $3a_4$ and $3b_4$). Whereas in the case of the $K\text{-}Zn_{0.4}Co_{2.6}O_4|Al_2O_3$ catalyst, potassium is distributed between the spinel and occasionally the alumina carrier surface, for the cesium doped samples, the alkali promoter is mainly confined to the spinel nanograins. Such behavior can be accounted for by the results of thermal alkali desorption studies. The results for potassium and cesium desorption from the investigated catalysts are shown in Fig. 4. They clearly reveal a difference in the thermal stability between these promoters. The onset for cesium desorption is observed at ~350 °C while in the case of potassium it is shifted to ~500 °C. A clear exponential character of the desorption curve as a function of temperature implies that the desorption occurs

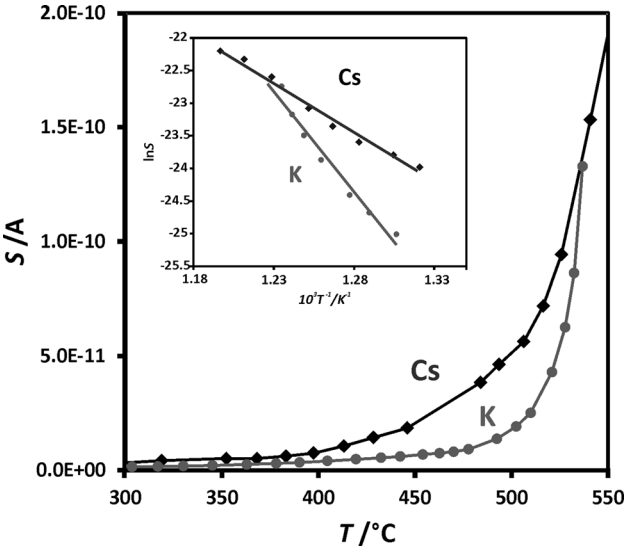

Fig. 4 Thermal desorption of Cs and K from the surface of the $Zn_{0.4}Co_{2.6}O_4|Al_2O_3$ catalyst together with the corresponding Arrhenius plots (*inset*)

through single barrier associated with the Cs–O_{surf} bond breaking. Indeed, the Arrhenius plot (shown in the insert) is linear in the investigated temperature range and the activation energy, equal to 1.3 eV, can be reliably determined. This value is characteristic of Cs atom desorption from the cobalt spinel surface at low coverages as shown and discussed in our previous paper [12]. In the case of potassium the desorption process is more complex as the Arrhenius plot reveals two desorption energies of 2.6 and 1.2 eV (at low temperature, shown in [8]). They can be associated with potassium desorption from the cobalt spinel phase and the alumina support. In conclusion, the microscopic and thermal desorption studies revealed consistently that potassium is distributed between the active phase (major part) and the support (minor part), while cesium is present mainly at the spinel phase.

The catalytic deN_2O activity of the two series of the potassium and cesium doped $Zn_{0.4}Co_{2.6}O_4|Al_2O_3$ samples of various alkali loadings was examined by means of the TPSR measurements. The results expressed as N_2O conversion versus temperature are collated in Fig. 5. The comparison of the N_2O conversion profiles for the K-doped (Fig. 5a) and Cs-doped (Fig. 5b) $Zn_{0.4}Co_{2.6}O_4|Al_2O_3$ catalysts reveals strong impact of the alkali promotion on the extent of the N_2O conversion. It is manifested by pronounced shifts of the conversion curves towards lower and higher temperatures upon doping. The highest activity was found for the samples with the potassium loading of 0.116 wt% (2 atoms per nm^2) and cesium loading of 0.086 wt% (1 atom per nm^2). It should be noted, however, that the samples with the highest surface concentration of potassium (5 K, 10 K) or cesium (4 Cs, 6 Cs) exhibit lower activity than the undoped $Zn_{0.4}Co_{2.6}O_4|Al_2O_3$ catalyst.

The results of catalytic activity expressed as temperature of 50% of conversion are plotted as a function of potassium and cesium loadings in Fig. 6a (alkali loading expressed in wt% determined from XRF) and Fig. 6b (alkali loading expressed as a surface coverage in atoms per nm^2, calculated based on total BET area). It can be inferred that for both series the doping with alkali (K or Cs) showed non-monotonous behavior with the minimum in the range of 0.5–3 atoms per nm^2 for potassium and 0.5–2 atoms per nm^2 for cesium. It is worth to mention, that for both alkali promoters the $T_{50\%}$ can be lowered down to $\sim$350 °C, shifting down thereby the activity window by $\sim$80 °C.

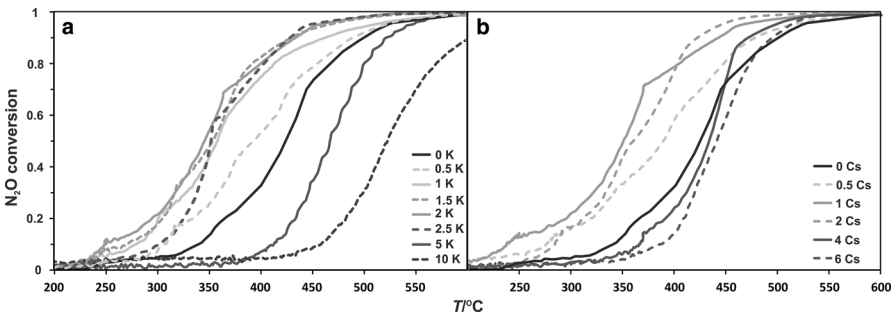

Fig. 5 The conversion curves for N_2O decomposition reaction over the $Zn_{0.4}Co_{2.6}O_4|Al_2O_3$ catalyst doped by **a** K and **b** Cs

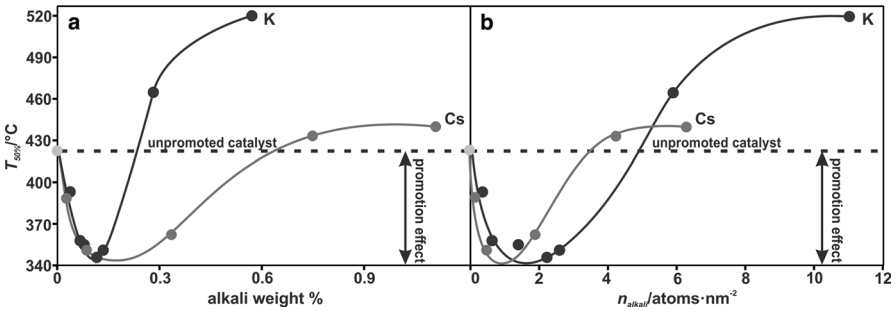

Fig. 6 The half conversion temperature changes as a function of alkali promoters loading (determined from XRF) of the $Zn_{0.4}Co_{2.6}O_4|Al_2O_3$ catalyst expressed in wt% (**a**) and as a surface coverage in atoms per nm^2 (**b**)

The beneficial effect of alkali promotion of bulk cobalt spinel was previously studied by work function measurements and DFT calculations [3]. Those studies allowed us to explain this effect in terms of electronic promotion gauged by a lowering of the catalyst work function and facilitation of the electron transfer from the catalyst surface to the reactant molecule, and thus N–O bond dissociation. As discussed therein, the alkali metals of low ionization potential ($IP_{Cs} = 3.89$ eV; $IP_K = 4.34$ eV) strongly modify the surface electronic properties of the catalyst. At low surface loadings, the deposited alkali form diffuse surface dipoles ($Cs^{\delta+}$–$O^{\delta-}_{surf}$ or $K^{\delta+}$–$O^{\delta-}_{surf}$) due to electron density donation to the spinel catalyst. Such dipoles counterbalance the surface electrostatic potential, facilitating electron shuttling between the catalyst and the N_2O reactant ($N_2O + e^-_{(Co)} \rightarrow N_2 + O^-_{surf}$) in the reduction step and the O^- intermediates ($2O^-_{surf} \rightarrow O_{2(g)} + 2e^-_{(Co)}$) in the oxidation step, that closes the catalytic cycle. The redox centers are constituted by the spinel octahedral cobalt ions [27]. However, when alkali surface coverage increases (alkali dipoles come closer) the beneficial effect of surface dipoles is ceasing due to the depolarization effect [28]. As a consequence, after passing the optimal loading, the activity falls down with the increasing alkali coverage (Fig. 6). It should be also noted that the negative effect at excessive coverages due to the large size of alkali cations may also results from the cobalt active sites blocking.

A comparison of the optimal level of alkali-doping for the supported spinel catalysts (0.5–2 for Cs and 0.5–3 for K) shows that they appreciably differ. This can be interpreted in terms of different surface stability of these both promoters and their surface dispersion (see microscopic observations). Although the activity enhancement is similar for these both promoters from practical point of view the superiority of potassium seems to be evident due to a considerably broader range of optimal loading and distinctly lower price of the promoter precursor. Thus, potassium addition should be much more easily to handle while upscaling the catalyst preparation for industrial applications. Another important point, speaking in favor of potassium, is its significantly higher thermal stability (the difference in the desorption onset between K and Cs reaches 150 °C, Fig. 4) in the temperature range of the catalyst practical operation for N_2O removal from the tail gases of nitric acid plants (350–450 °C).

Conclusions

A strong beneficial effect of potassium or cesium on the deN_2O activity of the $Zn_{0.4}Co_{2.6}O_4|Al_2O_3$ catalyst, gauged by the decrease in the $T_{50\%}$ by about 80 °C, was observed for both promoters at different optimal surface coverages (0.5–3 K atoms/nm^2 and 0.5–2 Cs atoms/nm^2). This founding was accounted for by a different surface stability of these both promoters and their dispersion on the catalyst surface. From a practical point of view, the superiority of potassium over cesium results from a broader range of the optimal loading and the much higher thermal stability in the temperature range of the catalyst practical operation for N_2O removal from the tail gases of nitric acid plants.

Acknowledgements The authors would like to acknowledge the Polish National Centre for Research and Development funding awarded by the decision number PBS2/A5/38/2013. The research was partially carried out with the equipment purchased thanks to the financial support of the European Regional Development Fund in the framework of the Polish Innovation Economy Operational Program (Contract No. POIG.02.01.00-12-023/08).

References

1. Pérez-Ramírez J, Kapteijn F, Schöffel K, Moulijin JA (2003) Formation and control of N_2O in nitric acid production: where do we stand today? Appl Catal B 44:117–151
2. Trogler WC (1999) Physical properties and mechanisms of formation of nitrous oxide. Coord Chem Rev 187:303–327
3. Zasada F, Stelmachowski P, Maniak G et al (2009) Potassium promotion of cobalt spinel catalyst for N_2O decomposition-accounted by work function measurements and DFT modelling. Catal Lett 127:126–131
4. Grzybek G, Stelmachowski P, Gudyka S et al (2016) Strong dispersion effect of cobalt spinel active phase spread over ceria for catalytic N_2O decomposition: the role of the interface periphery. Appl Catal B 180:622–629
5. Yan L, Ren T, Wang X et al (2003) Excellent catalytic performance of $Zn_xCo_{1-x}Co_2O_4$ spinel catalysts for the decomposition of nitrous oxide. Catal Commun 4:505–509
6. Yan L, Ren T, Wang X et al (2003) Catalytic decomposition of N_2O over $M_xCo_{1-x}Co_2O_4$ (M = Ni, Mg) spinel oxides. Appl Catal B 45:85–90
7. Abu-Zied BM, Soliman SA, Abdellah SE (2015) Enhanced direct N_2O decomposition over Cu_x-$Co_{1-x}Co_2O_4$ ($0.0 \leq x \leq 1.0$) spinel-oxide catalysts. J Ind Eng Chem 21:814–821
8. Grzybek G, Wójcik S, Legutko P et al (2017) Thermal stability and repartition of potassium promoter between the support and active phase in the K-$Co_{2.6}Zn_{0.4}O_4|\alpha$-$Al_2O_3$ catalyst for N_2O decomposition: Crucial role of activation temperature on catalytic performance. Appl Catal B 205:597–604
9. Karásková K, Obalová L, Kovanda F (2011) N_2O catalytic decomposition and temperature programmed desorption tests on alkali metals promoted Co-Mn-Al mixed oxide. Catal Today 176:208–211
10. Konsolakis M (2015) Recent advances on nitrous oxide (N_2O) decomposition over non-noble-metal oxide catalysts: catalytic performance, mechanistic considerations, and surface Chemistry aspects. ACS Catal 5:6397–6421

11. Stelmachowski P, Maniak G, Kotarba A, Sojka Z (2009) Strong electronic promotion of Co_3O_4 towards N_2O decomposition by surface alkali dopants. Catal Commun 10:1062–1065
12. Grzybek G, Stelmachowski P, Gudyka S et al (2015) Insights into the twofold role of Cs doping on deN_2O activity of cobalt spinel catalyst-towards rational optimization of the precursor and loading. Appl Catal B 168–169:509–514
13. Asano K, Ohnishi C, Iwamoto S et al (2008) Potassium-doped Co_3O_4 catalyst for direct decomposition of N_2O. Appl Catal B 78:242–249
14. Ohnishi C, Asano K, Iwamoto S et al (2007) Alkali-doped Co_3O_4 catalysts for direct decomposition of N_2O in the presence of oxygen. Catal Today 120:145–150
15. Pasha N, Lingaiah N, Babu NS et al (2008) Studies on cesium doped cobalt oxide catalysts for direct N_2O decomposition in the presence of oxygen and steam. Catal Commun 10:132–136
16. Maniak G, Stelmachowski P, Kotarba A et al (2013) Rationales for the selection of the best precursor for potassium doping of cobalt spinel based deN_2O catalyst. Appl Catal B 136–137:302–307
17. Inger M, Wilk M, Saramok M et al (2014) Cobalt spinel catalyst for N_2O abatement in the pilot plant operation-long-term activity and stability in tail gases. Ind Eng Chem Res 53:10335–10342
18. Boissel V, Tahir S, Koh CA (2006) Catalytic decomposition of N_2O over monolithic supported noble metal-transition metal oxides. Appl Catal B 64:234–242
19. Shen Q, Li L, Li J et al (2009) A study on N_2O catalytic decomposition over Co/MgO catalysts. J Hazard Mater 163:1332–1337
20. Christoforou SC, Efthimiadis EA, Vasalos IA (2002) Catalytic conversion of N_2O to N_2 over metal-based catalysts in the presence of hydrocarbons and oxygen. Catal Lett 79:137–147
21. Bueno-López A, Such-Basáñez I, de Lecea CSM (2006) Stabilization of active Rh_2O_3 species for catalytic decomposition of N_2O on La-, Pr-doped CeO_2. J Catal 244:102–112
22. Reddy PSS, Seshu Babu N, Pasha N et al (2008) Influence of microwave irradiation on catalytic decomposition of nitrous oxide over Rh/Al_2O_3 catalyst. Catal Commun 9:2303–2307
23. Gudyka S, Grzybek G, Gryboś J et al (2017) Enhancing the deN_2O activity of the supported $Co_3O_4|\alpha$-Al_2O_3 catalyst by glycerol-assisted shape engineering of the active phase at the nanoscale. Appl Catal B 201:339–347
24. Kotarba A, Rozek W, Serafin I, Sojka Z (2007) Reverse effect of doping on stability of principal components of styrene catalyst: $KFeO_2$ and $K_2Fe_{22}O_{34}$. J Catal 247:238–244
25. Kotarba A, Dmytrzyk J, Raróg-Pilecka W, Kowalczyk Z (2003) Surface heterogeneity and ionization of Cs promoter in carbon-based ruthenium catalyst for ammonia synthesis. Appl Surf Sci 207:327–333
26. Hadjiev VG, Iliev MN, Vergilov IV (1988) The Raman spectra of Co_3O_4. J Phys C 21:L199–L201
27. Stelmachowski P, Maniak G, Kaczmarczyk J et al (2014) Mg and Al substituted cobalt spinels as catalysts for low temperature deN_2O-Evidence for octahedral cobalt active sites. Appl Catal B 146:105–111
28. Somorjai GA (1993) Introduction to surface chemistry and catalysis. Wiley, New York